u!nnovation.

UNITED IMAGING

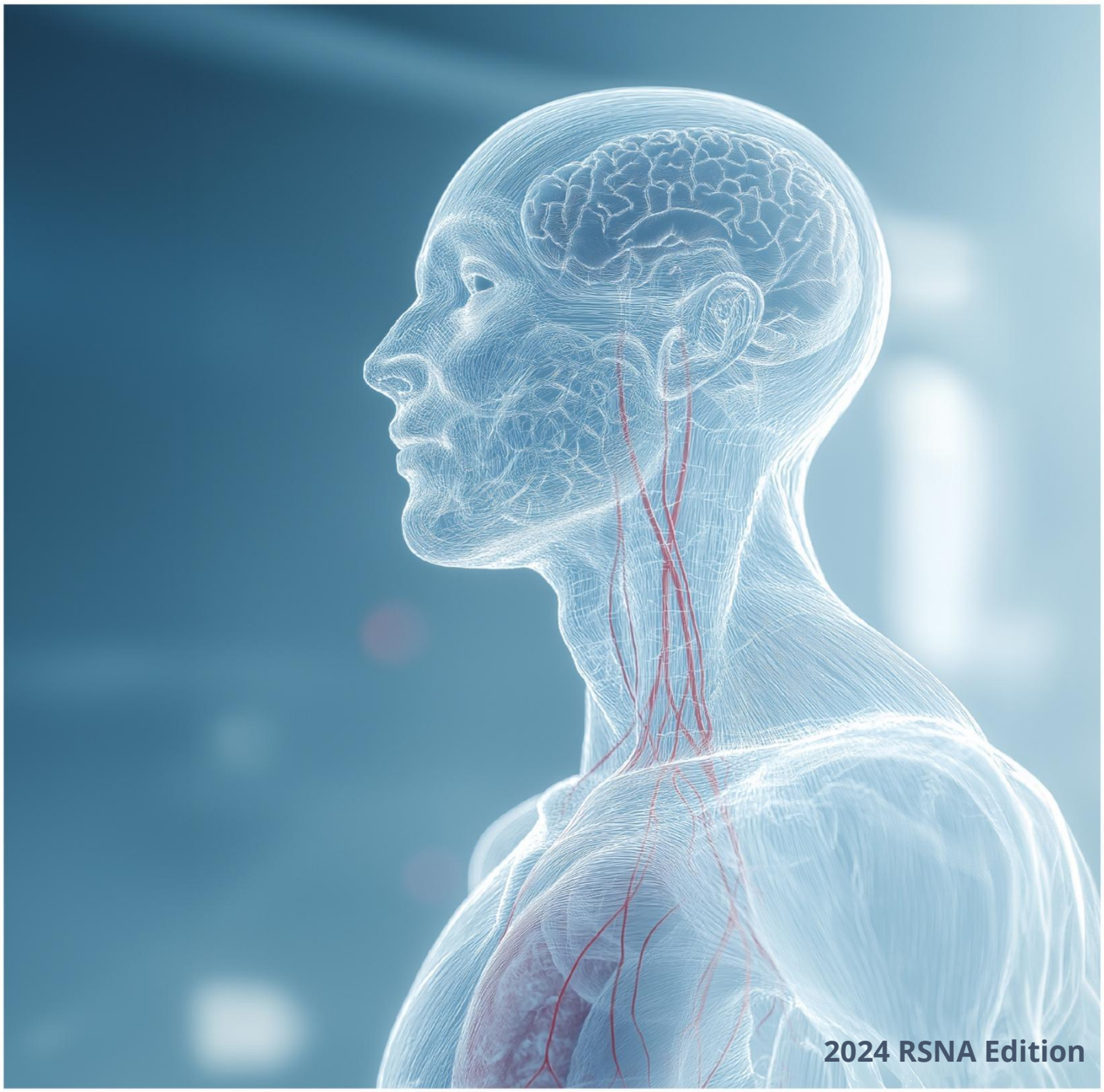

Issue Highlights

[Unveiling the Mind: Journeying through Brain PET with Dr. Richard E. Carson](#)

Edwin K. Leung

Page 25

[An AI-Empowered Head-Only Ultra-High-Performance Gradient MRI System for High Spatiotemporal Neuroimaging](#)

Liyi Kang et al.

Page 44

[5T MRI Compared to 3T MRI in Routine Brain Imaging: An Evaluation of Image Quality](#)

Zhensong Wang et al.

Page 53

[One-stop dynamic whole-brain CT perfusion with a 320-row scanner for patients with acute ischemic stroke and the clinical value of artificial intelligence iterative reconstruction](#)

Jin Fang et al.

Page 64

Disclaimer

The articles contained in this magazine are provided solely by the authors, and the author(s) of each article appearing in this magazine is/are solely responsible for the content thereof as well as personal data, which is used anonymously or complied with applicable data privacy laws or regulations. United Imaging Healthcare makes no representation or warranties, expressly or impliedly, with respect to the accuracy, timeliness, reliability, legitimacy, applicability, fitness, originality, or completeness of the contents of this magazine. United Imaging Healthcare assumes no legal responsibility or liability for any error, omission, or illegality with respect to the material contained within.

All articles contained in this magazine only represent the opinions and views of the authors and do not implicitly or explicitly represent any official positions or policies, or medical opinions of United Imaging Healthcare or the institutions with which the authors are affiliated unless this is clearly specified. Discussions of any brand, services, or products in the magazine should not be construed as promotion or endorsement thereof.

Articles published in this magazine are intended to inspire further general scientific research, investigation, understanding, and discussion only and are NOT intended to and should not be relied upon as recommending or promoting a specific medical advice, method, diagnosis, or treatment by physicians for any particular individual, nor to replace the advice of a medical doctor or other healthcare professional. Any individual wishing to apply the information in this magazine for the purposes of improving their own health should not do so without consulting with a qualified medical practitioner. All patients need to be treated in an individual manner by their personal medical advisors. The decision to utilize any information in this magazine is ultimately at the sole discretion of the reader, who assumes full responsibility for any and all consequences arising from such a decision. United Imaging Healthcare makes no representations or warranties with respect to any treatment, action, or application of medication or preparation by any person following the information offered or provided within or through the magazine. United Imaging Healthcare shall remain free of any fault, liability, or responsibility for any loss or harm, whether real or perceived, resulting from the use of information in this magazine.

The articles included in this magazine may contain work in progress, which represents ongoing research and development. Such technologies are not available for sale in the United States for clinical use and also may not be available for such sales in other countries around the world.

Please note that the magazine is intended to be distributed only within a limited scope instead of publication.

If you have any questions about the magazine, or simply wish to reach out to us for any other reasons, you are welcomed to contact us at the following email address: compliance@united-imaging.com

5T MRI Compared to 3T MRI in Routine Brain Imaging: An Evaluation of Image Quality

Zhensong Wang[1], Jianxian Liu[1], Zhengyi Li[1], Xin Wang[1], Zhangzhu Li[1], Yuan Guo[1], Dan Yu[2], Jie Gan[1,*]
[1] Department of Radiology, Shandong Provincial Third Hospital: Shandong University Affiliated Shandong Provincial Third Hospital, China
[2] United Imaging Research Institute of Intelligent Imaging, Beijing, China
* Corresponding author

1. Introduction

Ultra-high field Magnetic Resonance Imaging (MRI), defined as systems with main magnetic field strengths exceeding 3T, offers significant advantages over conventional clinical magnets. With comparable imaging parameters, ultra-high field MRI can deliver a higher signal-to-noise ratio (SNR), enabling higher spatial resolution and diminished partial volume effects, thereby enhancing the depiction of intracranial pathologies (1). Research comparing 7T with 3T MRI has highlighted the superiority of the former in visualizing cerebral small vessel diseases, multiple sclerosis, subtle anatomical abnormalities, and lesions associated with temporal lobe epilepsy (2). Furthermore, by optimizing the parameters of the relevant scanning sequence, such as the T2*-weighted gradient echo sequence, the contrast-to-noise ratio (CNR) is also observed to increase with an augmentation in field strength (1). Notably, ultra-high field MRI facilitates clearer visualization of anatomical structures like the amygdala, hippocampus, and substantia nigra, along with their subregions, as CNR improves (3, 4). Functional MRI (fMRI) at these field strengths can even resolve signals from distinct neuronal columns and layers (5). Consequently, ultra-high field MRI provides an abundance of morphological, functional, metabolic, and biochemical information about the brain (2, 6-11), attributable to its superior spatial and contrast resolutions.

Theoretically, both 5T and 7T MRI should produce images with higher SNR and CNR compared to 3T MRI (12, 13). In particular, studies have demonstrated that 5T time-of-flight magnetic resonance angiography (TOF MRA) outperforms 3T in subjective and objective assessments of distal large and small vessel branch visualization, with image quality comparable to 7T (14). Additionally, the use of a 48-channel orthogonal head coil at 5T mitigates radiofrequency (RF) pulse non-uniformity compared to 7T, facilitating the acquisition of high-quality brain images; this holds significant clinical potential. Currently, 5T clinical research is limited. This study aims to compare quantitative and qualitative parameters (SNR, CNR, artifacts, gray/white matter clarity, image quality) of routine cranial sequences at 3T and 5T, using similar scanning sequences and duration, based on previous ultra-high field MRI studies.

2. Materials and Methods

2.1 Study Population

This prospective study was approved by the Institutional Review Board of Shandong Provincial Third Hospital (Approval No. KKLL-2023078), and written signed consents were obtained from all participants prior to each examination. Between July and December 2023, a total of 17 participants (7 males, 10 females; age: 31.94±15.34 years; range: 20-69 years) were recruited through advertisements. The participant pool comprised healthy volunteers and asymptomatic individuals with a history of ischemic cerebrovascular events. The exclusion criteria encompassed those with a history of intracranial aneurysm surgery, intracranial vascular stent placement, heart/respiratory failure, severe consciousness impairment, intracranial hemorrhage, MRI contraindications, or significant motion artifacts in images.

2.2 MRI examinations

All participants underwent both the 3.0T and 5.0T MRI examinations. The 5.0T MRI examinations were conducted using a prototype whole-body MRI scanner (uMR Jupiter®, United Imaging Healthcare) with a 48-channel orthogonal head coil, whereas the corresponding 3T data were acquired utilizing a 3T MRI scanner (Philips “Ingenia”CX, Best, The Netherlands) with a 24-channel receive head coil. Each participant completed clinical routine sequence imaging at both 5T and 3T within a 48-hour period, encompassing T2WI

(T2 Weighted Imaging), T1WI (T1 Weighted Imaging), T2_FLAIR (T2 fluid attenuated inversion recovery), and DWI (Diffusion Weighted Imaging) (Table 1).

2.3 Image Analysis

2.3.1 Quantitative Assessment

After completion of all data collection, images were transmitted to the PACS system (FABRIC2.0 & SYNAPSE4.1). Quantitative measurements were conducted twice, with a time interval of 14 days. All the qualitative analyses were performed by two experienced radiologists with more than 15 years' experience. Two observers were blinded to both the MRI protocols and field strength, and independent measurements within predefined regions of interest (ROIs) were conducted to calculate SNR and CNR, ensuring unbiased quantitative outcomes.

The predefined ROIs encompassed the gray matter of the bilateral frontal lobes at the level of the semioval centers, along with their adjacent subcortical white matter; the bilateral putamen; and the central pons, bilateral cerebellums, and at the level of the middle cerebellar peduncles. SNR and CNR were calculated as follows:

$$SNR = SI/SD$$

$$CNR_{WM/GM} = (SI_{WM} - SI_{GM})/SD_{WM}$$

Where SI is the average signal intensity of brain white/gray matter, and SD is the standard deviation of these intensities within the tissue.

2.3.2 Subjective Assessment

Subjective evaluations were conducted by the same two radiologists, and were also repeated twice within a 14-day interval to ensure consistency. The assessments focused on three MR image index scores: artifacts (5 = no artifacts, 4 = minimal artifacts, 3 = slight artifacts, 2 = moderate artifacts, and 1 = very severe artifacts and non-diagnostic), gray-white matter definition (3 = Clear, 2 = boundary vague, 1 = non-distinguishable), overall image quality (4 = excellent quality, 3 = mild impact on diagnosis, 2 = substantial impact on diagnosis, 1 = non-diagnostic).

2.4 Statistical Analysis

Statistical analyses were performed using SPSS version 27. Qualitative assessment indices (image artifacts, gray-white matter definition, overall image quality) scores of each sequence image of 3.0T and 5.0T were compared by Wilcoxon rank sum tests. P values ≤ 0.05 were considered to be statistically significant for differences between the two groups.

The interobserver agreement of subjective SNR and CNR evaluations was quantified by intraclass correlation coefficients (ICCs). The interobserver agreement was considered to be poor for ICCs = 0.0–0.2, fair for ICCs = 0.2–0.4, moderate for ICCs = 0.4–0.6, substantial for ICCs = 0.6–0.8, and excellent for ICCs = 0.8–1.0. Subjective assessment indicator scores of interobserver agreement were statistically compared by Kappa consistency analysis (0–0.2, slight agreement; 0.21–0.4, fair agreement; 0.41–0.60, moderate agreement; 0.61–0.8, substantial agreement; > 0.8, excellent agreement).

3. Results

In the T2WI and T1WI sequences, the SNR of frontal lobe gray matter at the level of the semioval center, frontal lobe white matter at the level of the semioval center, putamen, pons, and middle cerebellar peduncles all demonstrated the superiority of 5T over 3T (P<0.001). In quantitative measurements of T2_FLAIR, there was a statistically significant difference in SNR of the putamen between the two field strengths (P<0.001), with a lower value in 5T.

There were no significant differences in SNR between 5T and 3T for frontal lobe gray matter at the level of the semioval center, frontal lobe white matter at the level of the semioval center, pons, and middle cerebellar peduncles, although SNR in the pons was slightly lower in 5T. In the T1WI sequence, there was no significant difference in CNR between gray and white matter at the level of the semioval center, with a slightly lower value in 5T (P=0.197). In both T2WI and T2_FLAIR, 5T exhibited higher CNR for gray and white matter at the level of the semioval center compared to 3T. (P<0.001) (Table 2).

Regarding the overall image quality scores, 5T demonstrated superior performance compared to 3T in the T1WI(P=0.006), T2WI (P=0.007), DWI (P=0.041), and T2_FLAIR (P=0.008) sequences (Table 4). For image artifacts, the 3T images in the DWI sequence exhibited significantly more artifacts than the 5T images (P=0.014), particularly in the regions adjacent to the frontal sinus and temporal bone (Figure 2, Table 4). There

were no significant differences in the degree of image artifacts between the two field strengths in the T2WI (P=0.382), T1WI (P=0.104), and T2_FLAIR (P=0.668) sequences (Table 4). The clarity of gray and white matter scores indicated that 5T images were significantly better than 3T images in the DWI (P<0.001) and T2_FLAIR (P=0.007) sequences. However, there were no significant differences between 5T and 3T images in the T1WI (P=0.332) and T2WI (P=0.332) sequences (Table 4).

Intraclass correlation coefficient (ICC) analysis demonstrated moderate to high levels of consistency in the SNR and CNR values of the 5T image sequences and 3T image sequences of intraobserver (Table 3). Kappa consistency analysis revealed moderate to high levels of consistency in the mean scores of interobserver qualitative assessment indicators (image artifacts, gray-white matter definition, overall image quality) for both the 5T and corresponding 3T image sequences (Table 5).

4. Discussions

High-resolution MRI of the central nervous system enables more precise localization of lesions (15) and depiction of their characteristics. This is particularly crucial for a variety of craniocerebral diseases such as multiple sclerosis (MS), temporal lobe epilepsy, cerebrovascular diseases, and tumors. In the case of MS, high-resolution MRI provides detailed insights into the relationship between plaques and blood vessels, iron deposition, and the dynamic evolution of pathological changes over time (16-18). Furthermore, it offers valuable information about microvascular structures in gliomas (19). By generating more detailed images, high-resolution MRI assists doctors in more accurately understanding the nature and location of lesions, thereby facilitating more precise diagnoses and the development of personalized treatment plans. Studies have shown that the central nervous system exhibits exceptional resolution on ultra-high field MRI (3). In certain applications, its spatial resolution can attain 100-200μm, enabling the observation of microstructures, functions, and molecular metabolism within the human body (20).

This study compares the quantitative and qualitative parameters (SNR, CNR, overall image quality, image artifacts, and gray-white matter clarity) of routine cranial sequences between 5T and 3T MRI, using similar scanning sequences and approximately the same scanning duration. The results demonstrate that without increasing scanning time and while enhancing spatial resolution (see Table 1), the SNR of the frontal lobe gray matter, frontal lobe white matter, putamen, pons, and middle cerebellar peduncle in the 5T T2WI and T1WI sequences is superior to that of 3T (P<0.001). This finding is consistent with a recent study on 5T-MRI (14). Numerous high-field MRI studies have also shown varying degrees of increased SNR compared to 3T (4, 21). SNR is a crucial metric for evaluating MRI images. Traditional theory, based on the Boltzmann distribution, suggests that as the magnetic field strength (B0) increases, the difference in the number of protons in low and high energy states increases proportionally. Moreover, the Larmor frequency (ω0) increases with B0, resulting in an increase in the dipole magnetic moment and thus the signal intensity (SI) collected by the coil, which is proportional to $B0^2$ ($SI \propto B0^2$). Considering that noise (N) is also proportional to B0, it was initially derived that SNR is proportional to B0 ($SNR \propto B0$) (22). However, the currently accepted relationship between SNR and B0 in ultra-high field strengths indicates a more exponential than linear relationship, with $SNR \propto B01.65$ (23). In this study, the greatest SNR improvement was observed in the frontal lobe gray matter of the T1WI sequence, whereas the smallest increase was noted in the middle cerebellar peduncle of the same sequence, with 5T SNR values approximately 1.9 times and 1.2 times those of 3T, respectively. These results do not entirely align with previous perspectives. Studies indicate that B0 uniformity significantly impacts SNR in high field strengths, and this uniformity diminishes as field strength increases (23), resulting in variations in radiofrequency (RF) excitation intensity across distinct regions and consequently influencing SNR. Additionally, the uniformity of the RF field decreases with increasing B0 (24). When B0 significantly exceeds 1.5T, wavelength effects in the RF field distribution complicate MR performance, leading to SNR losses (23, 25). Studies have shown that SNR is relatively uniform in the cranium at lower field strengths (e.g., 3.0T), but as field strength increases (e.g., 7.0T), wavelength effects lead to a reduction in SNR uniformity, which becomes more pronounced with increasing field strength. This is manifested as higher SNR at the periphery and lower SNR at the center of cranial images (23).

Table1 Parameters for 5T/3T scanning

	T2W	T1W	T2W_FLAIR	DWI
5 Tesla				
Repetition time (TR)	4200ms	2300ms	9000ms	3284ms
Echo time (TE)	105.12ms	16ms	140.4ms	61.4ms
Field of view（FOV）	230mm×200mm	230mm×200mm	230mm×200mm	230mm×230mm
Image matrix	544×100	384×100	352×100	256×100
Slice thickness	5mm	5mm	5mm	5mm
Number of slices	19	19	19	19
Flip angle (FA)	90°	90°	90°	90°
Acquisition time	2:02min	3:04min	3:18min	2:11min
Pixel resolution in plane	0.42mm×0.42mm	0.65mm×0.65mm	0.65mm×0.65mm	0.9mm×0.9mm
3 Tesla				
Repetition time (TR)	4200ms	2000ms	9000ms	3000ms
Echo time (TE)	105ms	20ms	120ms	86ms
Field of view（FOV）	230mm×200mm	230mm×199mm	230mm×199mm	230mm×230mm
Image matrix	384×313	304×250	308×209	162×162
Slice thickness	5mm	5mm	5mm	5mm
Number of slices	19	19	19	19
Flip angle (FA)	90°	90°	90°	90°
Acquisition time	2:14min	3:04min	3:09min	2:04min
Pixel resolution in plane	0.64mm×0.64mm	0.76mm×0.80mm	0.76mm×0.95mm	1.42mm×1.42mm

Table 2. Statistical results of SNR and CNR for different sequences in 5T and 3T MRI

	5T	3T	t	P
T2WI				
Gray matter SNR (centrum semiovale level)	33.96±5.60	25.16±4.04	4.845	<0.001
White matter SNR (centrum semiovale level)	37.53±5.62	26.55±4.72	6.013	<0.001
Gray-white matter CNR (centrum semiovale level)	14.81±3.46	8.53±2.94	9.220	<0.001
Putamen SNR	27.67±4.83	19.26±4.55	7.590	<0.001
Pons SNR	22.19±3.64	15.43±2.97	7.428	<0.001
Cerebellar peduncle SNR	30.06±4.73	22.05±4.06	7.029	<0.001
T1WI				
Gray matter SNR (centrum semiovale level)	35.93±6.11	18.95±3.39	9.639	<0.001
White matter SNR (centrum semiovale level)	65.20±9.49	49.29±7.7.38	6.408	<0.001
Gray-white matter CNR (centrum semiovale level)	19.31±3.84	21.30±4.08	-1.346	0.197
Putamen SNR	37.28±5.17	27.03±5.10	8.528	<0.001
Pons SNR	32.03±5.33	23.65±4.99	4.793	<0.001
Cerebellar peduncle SNR	40.21±5.45	31.54±5.83	5.769	<0.001
T2_FLAIR				
Gray matter SNR (centrum semiovale level)	41.69±8.01	39.87±6.21	0.711	0.487
White matter SNR (centrum semiovale level)	40.33±6.43	38.81±10.38	0.462	0.650

Gray-white matter CNR (centrum semiovale level)	11.24±3.48	5.52±2.42	9.181	<0.001
Putamen SNR	24.89±4.85	29.84±6.36	-4.596	<0.001
Pons SNR	20.42±3.85	22.37±4.90	-1.471	0.161
Cerebellar peduncle SNR	31.73±5.86	29.62±4.35	1.178	0.256

Table 3. Statistical results of subjective evaluation for 5T and 3T MRI

	5T (Mean ± SD)	**3T (Mean ± SD)**	**P**
Overall image quality			
T1W_FLAIR	3.82±0.85	3.47±0.37	0.006
T2WI	3.94±0.16	3.50±0.58	0.007
DWI	4.00±0.00	3.76±0.43	0.041
T2W_FLAIR	3.82±0.35	3.41±0.30	0.008
Artifacts			
T1W_FLAIR	3.70±0.46	3.47±0.51	0.104
T2WI	4.41±0.44	4.32±0.35	0.382
DWI	3.88±0.21	3.38±0.33	0.014
T2W_FLAIR	4.17±0.24	4.11±0.54	0.668
Gray-white matter clarity			
T1W_FLAIR	3.00±0.00	2.97±0.12	0.332
T2WI	3.00±0.00	2.94±0.24	0.332
DWI	3.00±0.00	2.32±0.30	<0.001
T2W_FLAIR	3.00±0.00	2.76±0.31	0.007

Table 4. ICC analysis results for 5T and 3T MRI sequences

	ICC		**95% CI**		**P**	
	5T-MRI	**3T-MRI**	**5T-MRI**	**3T-MRI**	**5T-MRI**	**3T-MRI**
T2WI						
Gray matter SNR (centrum semiovale level)	0.950	0.803	0.867,0.982	0.536,0.924	<0.001	<0.001
White matter SNR (centrum semiovale level)	0.877	0.892	0.693,0.954	0.728,0.960	<0.001	<0.001
Gray-white matter CNR (centrum semiovale level)	0.919	0.892	0.790,0.970	0.729,0.960	<0.001	<0.001
Putamen SNR	0.574	0.899	0.144,0.821	0.745,0.962	0.006	<0.001
Pons SNR	0.900	0.873	0.747,0.963	0.686,0.952	<0.001	<0.001
Cerebellar peduncle SNR	0.906	0.845	0.760,0.965	0.622,0.941	<0.001	<0.001
T1WI						
Gray matter SNR (centrum semiovale level)	0.764	0.665	0.460,0.908	0.285,0.264	<0.001	0.001
White matter SNR (centrum semiovale level)	0.847	0.817	0.629,0.942	0.564,0.930	<0.001	<0.001
Gray-white matter CNR (centrum semiovale level)	0.523	0.752	0.072,0.796	0.432,0.903	0.013	<0.001
Putamen SNR	0.888	0.819	0.718,0.958	0.568,0.930	<0.001	<0.001
Pons SNR	0.906	0.858	0.760,0.965	0.651,0.946	<0.001	<0.001

Cerebellar peduncle SNR	0.932	0.924	0.823,0.975	0.803,0.972	<0.001	<0.001
T2WI_FLAIR						
Gray matter SNR (centrum semiovale level)	0.777	0.673	0.485,0.913	0.300,0.868	<0.001	0.001
White matter SNR (centrum semiovale level)	0.815	0.890	0.560,0.929	0.722,0.959	<0.001	<0.001
Gray-white matter CNR (centrum semiovale level)	0.881	0.878	0.702,0.955	0.695,0.954	<0.001	<0.001
Putamen SNR	0.909	0.926	0.769,0.966	0.808,0.972	<0.001	<0.001
Pons SNR	0.748	0.798	0.430,0.901	0.527,0.922	<0.001	<0.001
Cerebellar peduncle SNR	0.917	0.754	0.787,0.969	0.442,0.903	<0.001	<0.001

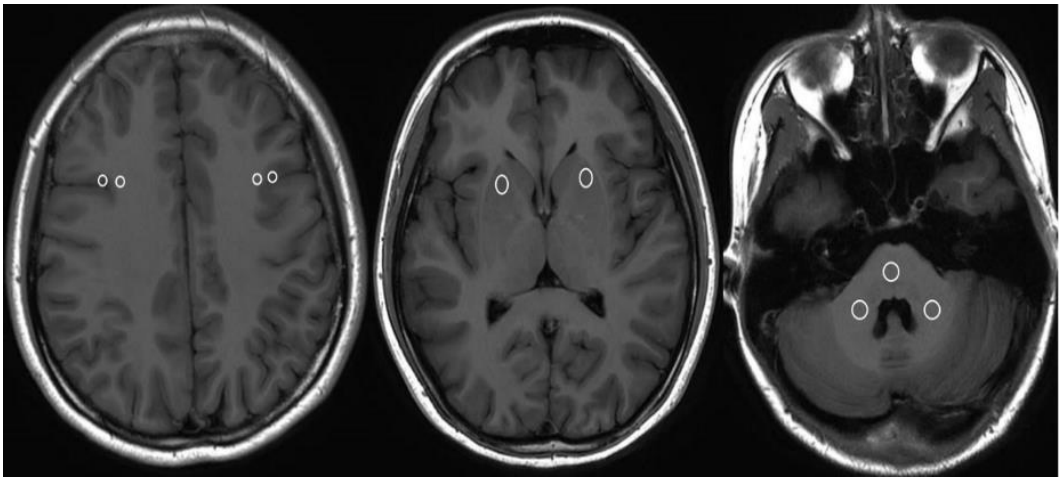

Figure 1. Placement of the regions of interest (ROI). 1a: Gray matter of the frontal lobe and adjacent subcortical white matter at the level of the bilateral centrum semiovale (ROI size: 5-8 mm^2). 1b: Bilateral putamen (ROI size: 20-30 mm^2). 1c: Central pons, bilateral cerebellum, and cerebellar peduncles at the same level (ROI size: 20-30 mm^2).

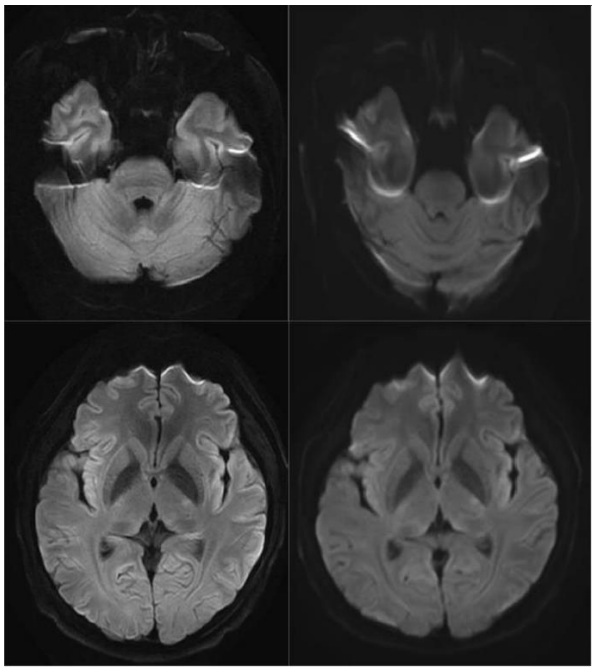

Figure 2. Reduced distortion caused by susceptibility artifacts in the frontal sinus and temporal bone regions in the 5T images compared to the 3T images. 2a, 2b: DWI images of the same participant. 2c, 2d: DWI images of the same participant. 2a, 2c were acquired using a 5T scanner, and 2b, 2d were acquired using a 3T scanner. The images show reduced distortion caused by susceptibility artifacts in the frontal sinus and temporal bone regions in the 5T images compared to the 3T images.

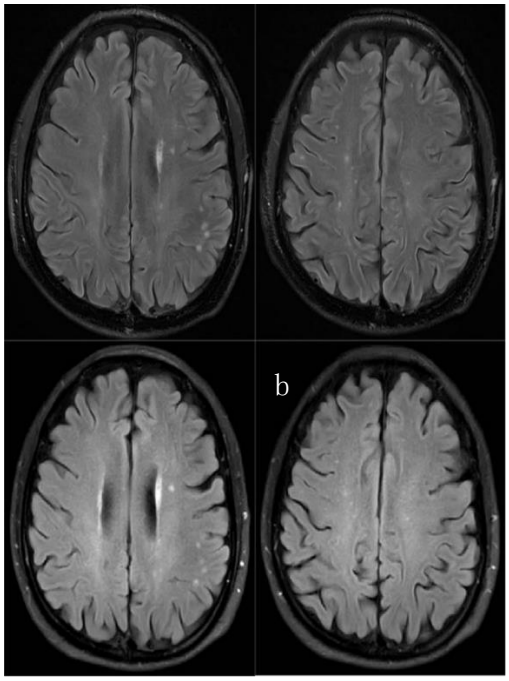

Figure 3. 5T images reveal a greater number of lesions and display clearer lesion boundaries compared to the 3T images. 3a, 3c: T2-FLAIR images of the same participant. 3b, 3d: T2-FLAIR images of the same participant.3a, 3b were acquired using a 5T scanner, and 3c, 3d were acquired using a 3T scanner.

Furthermore, SNR is also influenced by factors such as scanning sequences and tissue relaxation characteristics. Studies have shown that as magnetic field strength increases, tissue T1 values increase and T2 values decrease, SNR continues to elevate with magnetic field strength, albeit at a rate lower than linear, while tissue T1 contrast decreases and T2 contrast increases (26). Therefore, in high-field imaging, imaging sequence TR and TE need to be optimized (e.g., moderately extended) to achieve the best T1/T2 contrast. In this study, to enhance T1 contrast, the TR time of the high-field T1WI sequence was extended by 300 ms compared to 3T. In addition, SNR is closely tied to the coil type (23), where multi-channel surface coils facilitate super-linear SNR enhancements, whereas volume coils exhibit marginally sub-linear SNR gains. Regarding the T2_FLAIR sequence, no significant differences in SNR were observed between the two field strengths in frontal lobe gray matter, frontal lobe white matter, pons, and middle cerebellar peduncle. Intriguingly, SNR in the putamen was notably lower at 5T compared to 3T ($P<0.001$), a finding congruent with a recent study contrasting various field strengths (5T vs 7T) (14). Apart from the previously mentioned factors, this discrepancy might stem from the elevation of tissue T1 values accompanying the increase in B0 (23), as well as reduction in the transverse magnetization vector (Mxy) during the TR interval. Besides, considerations should be given to: (1) the shortened T2 relaxation time and subsequent faster signal attenuation due to age-related physiological iron deposition in the putamen; and (2) the higher spatial resolution at 5T. Consequently, in clinical practice, changes in the SNR of MRI images are anticipated to be more intricate than theoretically predicted (24).

Both T2WI and T2_FLAIR sequences showed superior CNR in the frontal lobe gray and white matter at 5T compared to 3T ($P<0.001$). These results are consistent with numerous ultra-high field MRI studies, which indicate that both 5T and 7T provide higher CNR than 3T (12-14). This superiority may be related to the following factors: 1) the augmentation of magnetic field strength B0 enhances the intensity of magnetic resonance signals. Consequently, when the signal intensities of two different tissues both increase, the difference in signal intensity between them also increases, while the increase in noise is relatively smaller; 2) as B0 increases, T2 values decrease (23), and increasing TE can enhance T2 contrast. Conversely, in the T1WI sequence, there was no significant difference in CNR between the two field

strengths for frontal lobe gray and white matter (P=0.197), with a marginally lower value observed at 5T. This observation is in accordance with a recent study investigating CNR at varying field strengths (Zhang S hi et al., 2023). This outcome may be attributed to the moderate prolongation of TR in ultra-high field strengths, which leads to elevated T1 values and diminished differences among various tissues (23). The overall image quality scores indicated that 5T was superior to 3T, suggesting that the higher spatial resolution and good SNR and CNR achievable at ultra-high field 5T, without increasing scanning time, can provide more detailed intracranial anatomical and pathological information and enable the detection of small lesions that are undetectable by lower field MRI. In this study, one participant showed significantly more white matter high signal intensity at 5T than at 3T (see Figure 2), with clearer lesion boundaries. This observation may be attributed to the enhanced image spatial resolution and improved tissue contrast at 5T. Nevertheless, as field strength escalates, magnetic susceptibility effects and chemical shift phenomena become more sensitive. Additionally, the diminished uniformity of the B0 and RF fields owing to the heightened field strength can significantly compromise image quality at tissue interfaces. For example, brain tissue proximal to the frontal sinus and temporal bone exhibits distortion and warping (see Figure 3). To address this issue, the present study employed a 48-channel orthogonal head coil at 5T, which significantly mitigated RF inhomogeneity, thereby substantially enhancing central nervous system imaging quality and reduced artifact (27-29). Secondly, the application of the multi-shot EPI sequence, with multiple RF excitations, shorter TE, and segmented multiple filling of K-space, contributed to the amelioration of magnetic susceptibility artifacts. Furthermore, this might also be related to the higher stability of the 5T magnetic field uniformity, gradient system, and RF system. Based on these factors, magnetic susceptibility artifacts in the DWI sequence were significantly reduced at 5T compared to 3T. In the assessment of gray-white matter clarity, 5T images from the T1WI and T2WI sequences were not significantly different from those of 3T, while the T2-FLAIR and DWI sequences showed significantly better performance at 5T.

This is consistent with the increased CNR values in the T2-FLAIR sequence at 5T, which enhances gray-white matter contrast. It should be noted that in conventional 3T MRI, the depiction of small lesions is hindered by several factors in the DWI sequence, including limited spatial resolution, convoluted K-space filling patterns, the absence of corrective measures during image acquisition, and prominent magnetic susceptibility artifacts. For instance, it is prone to missed diagnoses or misdiagnoses of MS cortical lesions, epileptogenic foci, and structural changes in the hippocampus in patients with dementia and Parkinson's disease.

Therefore, in this study, the voxel size within the 5T layer was set smaller than that of the 3T layer (5T vs 3T: 0.90mm×0.90mm vs 1.42mm×1.42mm) to evaluate the image quality of the 5T MRI. The scoring results indicated that the overall image quality and the clarity of gray and white matter in the 5T images were superior to those in the 3T images (P=0.041; P<0.001). These findings can be attributed not only to the smaller pixel size and consequently higher spatial resolution in the 5T images, but also to factors such as the use of a multi-shot EPI sequence with multiple RF excitations, shorter TE, and segmented multi-filling of the K-space. Furthermore, the use of a 48-channel orthogonal head coil, along with the higher stability of the gradient and radiofrequency systems in the 5T MRI, contributed to these outcomes. Consequently, the results of this study suggest that in ultra-high field DWI sequences, it is feasible to achieve higher spatial resolution while maintaining a certain level of SNR.

This study demonstrates moderate to high consistency in the ICC values of SNR and CNR across various sequences (excluding DWI) at 5T and 3T, as well as in the Kappa values for qualitative assessment metrics (image artifacts, gray-white matter definition, overall image quality) at both field strengths (see Tables 4-6, 8-10). These findings indicate the robustness and reproducibility of the study results. However, the study cohort comprised solely healthy volunteers or asymptomatic individuals with a history of ischemic cerebrovascular events, thus limiting the generalizability of 5T's efficacy in specific intracranial pathologies. Future research should validate these findings in relevant cranial lesion populations.

The results suggest that within similar scan times, 5T MRI provides higher spatial resolution and improved tissue contrast, thereby laying a solid technological foundation for precise localization and detailed information acquisition in

cranial diseases. Further clinical applications require optimization of sequences to obtain better image data. It is worth mentioning that participants did not experience significant discomfort after the examination, contrasting with previous reports of vertigo in 7T studies (2). This discrepancy may be attributed to the study population.

The study recruited 17 participants for data collection, which constitutes a relatively small sample size for a cross-sectional study. Therefore, the results are presented as preliminary conclusions. Future research should expand the sample size to validate the study's findings. Additionally, as participants were asymptomatic, with only some older individuals showing ischemic infarcts on cranial MRI, the study does not fully demonstrate 5T-MRI's sensitivity to pathological changes. Thus, the focus of future research should be on assessing the lesion detection capabilities of ultra-high field 5T-MRI. Furthermore, the use of MR scanners from different manufacturers, different head coils, and varying sequence acquisition parameters may have influenced image SNR, CNR, and subjective assessment metrics. Moreover, the absence of acceleration techniques to isolate field strength effects resulted in longer overall scan times.

In conclusion, this study demonstrates that, within a comparable scanning duration, 5T MRI offers superior spatial resolution, along with enhanced SNR and CNR, conferring advantages in terms of overall image quality and definition of brain gray matter. Nonetheless, the escalation in field strength also results in an increase in T1 values, intensified inhomogeneity of the RF field, and heightened sensitivity to the chemical shift phenomenon. Consequently, optimizing scanning parameters in clinical settings is imperative to balance SNR, CNR, spatial resolution, and acquisition time, thereby ensuring optimal image quality and enhancing diagnostic accuracy.

5. References

1. Duyn JH, The future of ultra-high field MRI and fMRI for study of the human brain. Neuroimage (2012). 62, 1241–1248. http://dx.doi.org/10.1016/ j.neuroimage. 2011.10.065.
2. Springer E, Dymerska B, Cardoso PL, Robinson SD, Weisstanner C, Wiest R, Schmitt B, Trattnig S, Comparison of Routine Brain Imaging at 3T and 7T. Invest Radiol (2016). Aug; 51(8):469-82. doi: 10.1097/RLI.0000000000000256.
3. Thomas BP, Welch EB, Niederhauser BD, et al., High-resolution 7T MRI of the human hippocampus in vivo. J Magn Reson Imaging (2008). 28(5):1266-1272. DOI: 10.1002/jmri.21576.
4. Cho ZH, Lee YB, Kang CK, et al., Microvascular imaging of asymptomatic MCA steno-occlusive patients using ultra-high-field 7T MRI. J Neurol (2013). 260(1):144–150.
5. Yacoub E, Shmuel A, Pfeuffer J, Van De Moortele PF, Adriany G, Andersen P, Vaughan JT, Merkle H, Ugurbil K, Hu X, Imaging brain function in humans at 7T. Magn Reson Med (2001). 45, 588–594.
6. Trattnig S, Bogner W, Gruber S, et al., Clinical applications at ultrahigh field (7 T). Where does it make the difference? NMR in Biomedicine (2016). Sep; 29(9):1316-1334. DOI: 10.1002/nbm.3272.
7. Beisteiner R, Robinson S, Wurnig M, Hilbert M, Merksa K, Rath J, Hollinger I, Klinger N, Marosi C, Trattnig S, Geissler A, Clinical fMRI: evidence for a 7T benefit over 3T. NeuroImage (2011). 57, 1015–1021.
8. Goncalves NR, Ban H, Sanchez-Panchuelo RM, Francis ST, Schluppeck D, Welchman AE, 7T FMRI reveals systematic functional organization for binocular disparity in dorsal visual cortex. - J. Neurosci (2015). 35, 3056–3072.
9. Bogner W, Chmelik M, Andronesi OC, Sorensen AG, Trattnig S, Gruber S, In Vivo (31) P Spectroscopy by Fully Adiabatic Extended Image Selected In Vivo Spectroscopy: a Comparison Between 3T and 7T. Magn Reson Med (2011). 66, 923–930.
10. Biller A, Badde S, Nagel A, Neumann JO, Wick W, Hertenstein A, Bendszus M, Sahm F, Benkhedah N, Kleesiek J, Improved Brain Tumor Classification by Sodium MR Imaging: prediction of IDH Mutation Status and Tumor Progression. AJNR Am. J. Neuroradiol (2016). 37, 66–73.
11. Zaiss M, Windschuh J, Paech D, Meissner JE, Burth S, Schmitt B, Kickingereder P, Wiestler B, Wick W, Bendszus M,

Schlemmer HP, Ladd ME, Bachert P, Radbruch A, Relaxation-compensated CEST-MRI of the human brain at 7T: unbiased insight into NOE and amide signal changes in human glioblastoma. Neuroimage (2015). 112, 180–188.

12. Triantafyllou C, Hoge RD, Krueger G, et al., Comparison of physiological noise at 1.5T, 3T and 7T and optimization of fMRI acquisition parameters. Neuroimage (2005). 26(1):243–250.17.

13. Vizioli L, Moeller S, Dowdle L, et al., Lowering the thermal noise barrier in functional brain mapping with magnetic resonance imaging. Nat Commun (2021). 12(1):5181.

14. Zhang Shi, Xueying Zhao, Shuo Zhu, Xiyin Miao, Yunfei Zhang, Shihong Han, Bei Wang, Boyu Zhang, Xiaodan Ye, Yongming Dai, Caizhong Chen, Shengxiang Rao, Jiang Lin Mengsu Zeng, He Wang, Time-of-Flight Intracranial MRA at 3T versus 5T versus 7T: Visualization of Distal Small Cerebral Arteries. Radiology (2023). DOI: 10.1148/radiol. 220114.

15. van Veluw SJ, Zwanenburg JJ, Engelen-Lee J, et al., In vivo detection of cerebral cortical microinfarcts with high-resolution 7T MRI. J Cereb Blood Flow Metab (2013). 33:322–329.

16. Dal-Bianco A, Hametner S, Grabner G, et al., Veins in plaques of multiple sclerosis patients—a longitudinal magnetic resonance imaging study at 7Tesla. Eur Radiol (2015). 25:2913–2920.

17. Bagnato F, Hametner S, Yao B, et al., Tracking iron in multiple sclerosis: a combined imaging and histopathological study at 7Tesla. Brain (2011). 134: 3599–3612.

18. Absinta M, Sati P, Gaitán MI, et al., Seven-tesla phase imaging of acute multiple sclerosis lesions: a new window into the inflammatory process. Ann Neurol (2013). 74:669–678.

19. Di Ieva A, Göd S, Grabner G, et al., Three-dimensional susceptibility-weighted imaging at 7T using fractal-based quantitative analysis to grade gliomas. Neuroradiology (2013). 55:35–40.

20. Zidong Wei, Qiaoyan Chen, Shihong Han, Shuheng Zhang, Na Zhang, Lei Zhang, Haining Wang, Qiang He, Peng Cao, Xiaoliang Zhang, Dong Liang, Xin Liu, Ye Li, Hairong Zheng, 5T magnetic resonance imaging: radio frequency hardware and initial brain imaging. Quant Imaging Med Surg (2023). 13(5):3222-3240.

21. Grochowski C, Staśkiewicz G. Ultra high field TOF-MRA: A method to visualize small cerebral vessels. 7T TOF-MRA sequence parameters on different MRI scanners - Literature review. Neurol Neurochir Pol (2017). 51(5):411–418.

22. Collins CM, Smith MB, Signal-to-noise ratio and absorbed power as functions of main magnetic field strength, and definition of "90" RF pulse for the head in the birdcage coil. Magn Reson Med (2001). 45:684–691.

23. Pohmann R, Speck O, Scheffler K, Signal-to-noise ratio and MR tissue parameters in human brain imaging at 3, 7, and 9.4 T using current receive coil arrays. Magn Reson. Med (2016). 75,801–809.

24. Daniel Gallichan, Diffusion MRI of the human brain at ultra-high field (UHF): A review. NeuroImage (2018). DOI: 10.1016/j.neuroimage.

25. Hoult DI, Sensitivity and power deposition in a high-field imaging experiment. J Magn Reson Imaging (2000). 12:46–67.

26. Robin A. de Graaf, Peter B. Brown, Scott McIntyre, Terence W. Nixon, Kevin L. Behar, and Douglas L. Rothman, High Magnetic Field Water and Metabolite Proton T1 and T2 Relaxation in Rat Brain In Vivo. Magnetic Resonance in Medicine (2006). DOI: 10.1002/mrm.20946.

27. de Zwart JA, Ledden PJ, Kellman P, van Gelderen P, Duyn JH, Design of a SENSE-optimized high-sensitivity MRI receive coil for brain imaging. Magn Reson Med (2002). 47, 1218–1227.

28. Wiggins GC, Potthast A, Triantafyllou C, Wiggins CJ, Wald LL, Eightchannel phased array coil and detunable TEM volume coil for 7T brain imaging. Magn Reson Med (2005). 54, 235–240.

29. Wiggins GC, Triantafyllou C, Potthast A, Reykowski A, Nittka M, Wald LL, 32-channel 3T receive-only phased-array head coil with soccer-ball element geometry. Magn Reson Med (2006). 56, 216–223.

Author Biography

Prof. Jie Gan

Chief Physician at the Imaging Center

The Affiliated Hospital of Shandong University, China

Prof. Jie Gan is a Chief Physician at the Imaging Center of the Third Affiliated Hospital of Shandong University. He earned his Master's degree in Imaging Medicine and Nuclear Medicine from Shandong University in 2003 and his Bachelor's degree in Clinical Medicine from Shandong Medical University in 1993. Prof. Gan has accumulated extensive experience in the field of radiology over three decades. His research focuses on advanced multimodal imaging, including 5T MRI, to study lipid metabolism, atherosclerosis, and brain function in Type 2 diabetes. He has led several major projects funded by the Shandong Provincial Health Commission and has published widely in medical journals. Prof. Gan is recognized for his contributions to radiology and continues to innovate in MRI applications.

PASSION for CHANGE

If you have any questions about the magazine, or simply wish to reach out to us for any other reasons, you are welcomed to contact us at the following email address: compliance@united-imaging.com